Climate Dynamics
https://doi.org/10.1007/s00382-018-4467-x

Subseasonal atmospheric regimes and ocean background forcing of Pacific Arctic sea ice melt onset

Thomas J. Ballinger[1] · Cameron C. Lee[2] · Scott C. Sheridan[2] · Alex D. Crawford[3] · James E. Overland[4] · Muyin Wang[4,5]

Received: 13 March 2018 / Accepted: 23 September 2018

Abstract
One observed fingerprint of Pacific Arctic environmental change, induced by climate warming and amplified local feedbacks, is a shift toward earlier onset of sea ice melt. Shorter freeze periods impact the melt season energy balance with cascading effects on ecological productivity and human presence in the region. Through this study, a non-linear technique, self-organizing maps, is utilized to investigate the subseasonal role of regional pressure patterns and associated lower-tropospheric wind regimes on melt onset in the Beaufort and Chukchi Seas. Focus is directed on the frequency and duration (≥ 3 consecutive days) of offshore, onshore, and zonal/weak flow that tend to precede anomalous (late and early) and average times of melt. Background North Pacific climate forcing ascribed from the Pacific Decadal Oscillation (PDO) phase and Bering Strait oceanic heat flux measurements provide a surface thermal context to the composite wind fields. In early melt onset years, onshore (northerly) winds occur approximately 1–3 fewer days with offsetting increases in zonal and offshore flow in the Beaufort and Chukchi Seas. During these cases, the Beaufort High pattern tends to set-up more frequently around the southeastern Beaufort Sea region, yielding winds of a southerly and/or easterly nature that are enhanced by cyclone activity to the south or downstream. Chukchi Sea weather analyses, in particular, suggest that interacting, precursor mechanisms involving warm air advection off snow-free Arctic lands and from southerly latitudes coupled with a slightly positive PDO state and anomalous, poleward oceanic heat transfer condition the seasonal ice pack for increasingly early melt.

Keywords Sea ice · Melt onset · Pacific Arctic · Pacific Decadal Oscillation · Self-organizing maps

1 Introduction

Nearly four decades of passive microwave satellite observations have revealed substantial downward trends in Arctic sea ice coverage across the annual cycle (Simmonds 2015), though spatial patterns of loss at the marginal sea scale have not been homogenous (Peng and Meier 2018). Some of the greatest sea ice losses throughout summer have occurred in the Pacific sector of the Arctic, including the Beaufort and Chukchi Seas (Wang and Overland 2015; Comiso et al. 2017; Kashiwase et al. 2017; Fig. 1). Reductions in the region's ice cover are, in part, a function of ice-type transition from thicker multi-year ice to thinner seasonal ice, with this conversion particularly apparent in scatterometer-derived imagery since roughly 2000 (Kwok and Cunningham 2010; Polyakov et al. 2012; Wood et al. 2015).

The transformation to a seasonal ice pack, especially in shallow, coastal waters and southern boundaries of the aforementioned Pacific Arctic marginal seas, has coincided with a shift in ice phenology toward earlier melt onset (negative trends) and later freeze-up (positive trends) since 1979 (Markus et al. 2009; Stroeve et al. 2014). Considering the Beaufort region, Steele et al. (2015) remarked that while ice retreat dates have trended earlier across longitudinal cross-sections throughout the region (~ 150 – 120°W), the

Electronic supplementary material The online version of this article (https://doi.org/10.1007/s00382-018-4467-x) contains supplementary material, which is available to authorized users.

✉ Thomas J. Ballinger
tballinger@txstate.edu

[1] Department of Geography, Texas State University, 601 University Drive, San Marcos, TX 78666, USA

[2] Department of Geography, Kent State University, Kent, OH, USA

[3] Department of Geology, The College of Wooster, Wooster, OH, USA

[4] NOAA/PMEL, Seattle, WA, USA

[5] University of Washington/JISAO, Seattle, WA, USA

Published online: 27 September 2018

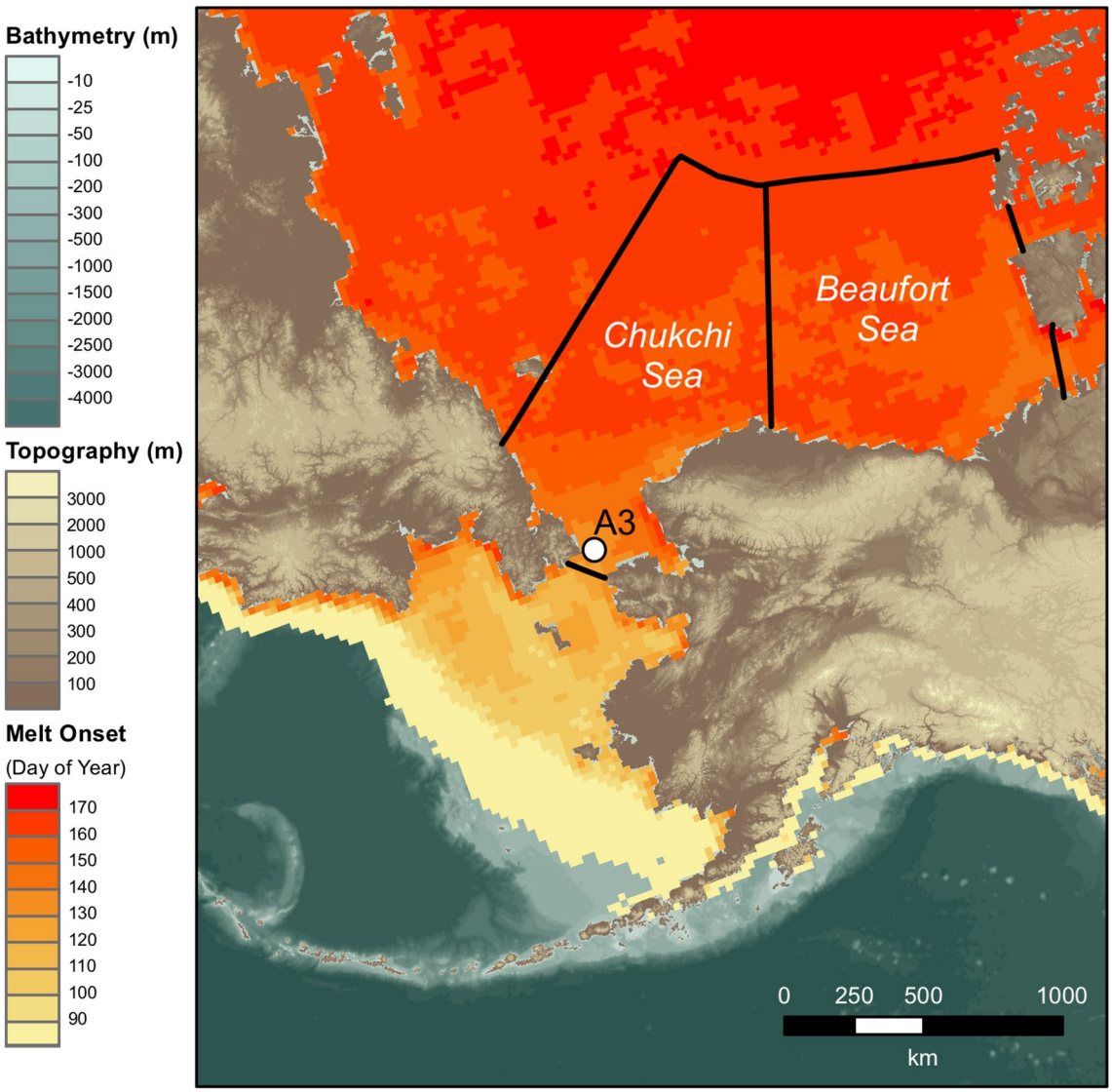

Fig. 1 Average dates of sea ice melt onset, 1979–2015, across the Pacific Arctic study region and adjacent waters. The Beaufort Sea and Chukchi Sea ice domains and the A3 mooring are identified within the map. Topography and bathymetry data are obtained from ETOPO1 (Amante and Eakins 2009)

most consistent and significant trends have occurred in the western half of the sea near the Chukchi boundary. Pan-Arctic melt onset trend maps (at 25 km pixel resolution and spanning the 1979–2013 period) from Stroeve et al. (2014; their Fig. 2a) show Chukchi and Beaufort waters largely undergoing a homogenous range of melt onset shifts on the order of 0–10 days earlier decade^{-1}. Multidecadal patterns of progressively earlier annual melt timing, yielding melt ponds on the sea ice as well as open water pockets within the pack, have allowed increased upper-ocean absorption of downward solar radiation, triggering earlier occurrence of the ice-albedo feedback process (Perovich et al. 2011; Stroeve et al. 2014; Wood et al. 2015).

This young, fragile ice cover is sensitive to a wide range of dynamic and thermodynamic forcing conditions (Serreze et al. 2016b). However, open water expansion during melt season ice edge retreat is often linked to the frequency, intensity, and duration of low-level (anti)cyclones traversing this portion of the Arctic basin, e.g. the summer 2007 persistent Beaufort High anomaly (L'Heureux et al. 2008; Ballinger and Sheridan 2014) and the strong early-to-mid-August cyclone of 2012 (Simmonds and Rudeva 2012). In addition to modulating solar heating of the upper-ocean, synoptic high pressure patterns also propagate Pacific inflow through Bering Strait, which affects melt processes of the Pacific marine Arctic (Wang et al. 2009; Woodgate et al. 2010).

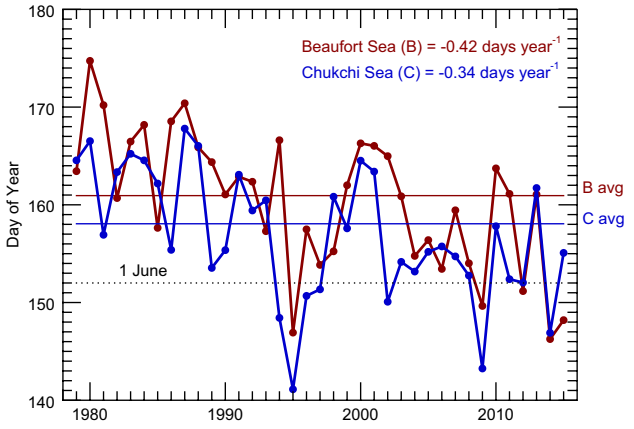

Fig. 2 Annual melt onset dates for the Beaufort and Chukchi Seas, 1979–2015. The Mann–Kendall trends shown (top right of figure) are both statistically significant ($p \leq 0.05$). Solid, colored horizontal lines depict average (avg) melt dates from the 19 years not falling within late or early melt onset bins (Table 2). The Julian day for 1 June (Day of Year 152), during non-leap years, is indicated for reference

Thus, an array of hydrologic and atmospheric mechanisms, local and remote, have recently been shown to affect characteristics of the Beaufort and Chukchi melt season (Wood et al. 2013; Ballinger and Rogers 2014; Nghiem et al. 2014; Ballinger and Sheridan 2015; Frey et al. 2015; Serreze et al. 2016a; Overland et al. 2018). However, relatively little is known about day-to-day atmospheric preconditioning factors that stimulate melt onset. Such observational information is increasingly valuable to sea ice forecasting improvements given ecosystem sensitivity to ice phenology shifts (Grebmeier et al. 2006) and increasing ship traffic and natural resource exploration over these waters (Eguíluz et al. 2016).

We present results from a subseasonal perspective to diagnose the frequency and duration of near-term atmospheric patterns and local and background oceanic conditions preceding the onset of Beaufort and Chukchi melt. Our analyses focus on surface to mid-level circulation and ocean/surface air temperature conditions rather than precursor ice pack dynamical processes associated with ice motion (e.g. ridging, rafting, lead formation) that are also known to influence spatial patterns of break-up. To synthesize results, we composite synoptic atmosphere and ocean states by early, average, and late melt events from the distribution of such cases across their respective time series. Our paper is outlined as follows: Sect. 2 covers dataset descriptions, Sect. 3 provides a methodological overview, Sect. 4 details our results, and a summary and discussion of our main findings are presented in Sect. 5.

2 Data

Passive microwave-derived brightness temperatures obtained from satellite products, including the Scanning Multichannel Microwave Radiometer and Special Sensor Microwave/Imager, are utilized in the creation of the Arctic melt onset dataset, 1979–2015 (see Markus et al. 2009 for processing algorithm details). Melt onset is defined as the average (sea-wide) day of year when above-freezing (skin or sea surface) temperatures occur, continuing until freeze onset later in the annual cycle, as evidenced by liquid water presence from melt ponds atop sea ice or ice-free open ocean conditions. Figure 1 shows the long-term mean melt onset dates across the Pacific Arctic sector and surrounding waters with the Beaufort and Chukchi Seas study areas outlined by thick black lines; corresponding regional melt onset time series are presented in Fig. 2.

Mean sea-level pressure (MSLP), 10-m vector wind fields (V_{10}), 925 hPa air temperatures (T925), and 500 hPa geopotential heights (GPH) are obtained from ERA-Interim (ERA-I) reanalysis (Dee et al. 2011) for the West Arctic region inclusive of the Beaufort and Chukchi Seas and terrestrial and coastal areas from 60 to 85ºN, 150ºE-70ºW. The 1200 UTC gridded fields at 1° latitude by 1° longitude horizontal resolution are analyzed in the study, for the years 1979–2015. ERA-I has been compared with other modern reanalysis products and is chosen for its performance characteristics in the Arctic marine environment (Zib et al. 2012; Ballinger et al. 2013; Lindsey et al. 2014). For example, 10-m winds exhibit low bias and high, positive correlation with observed North Pole drifting station winds during climatological spring (Lindsay et al. 2014). Winds at 10-m are also minimally affected by surface roughness from ice topography, which tends to extend < 2 m height from the surface over the Pacific Arctic seasonal ice zone (Petty et al. 2016). Daily data are obtained each year over a period from 1 March, the month of the climatological, pan-Arctic sea ice maximum (Simmonds 2015), to 30 June, the month of the latest melt onset dates for the marginal seas of interest to this study (Table 1).

Atmospheric analyses are supplemented with in situ Bering Strait oceanographic data to understand the local oceanic heat contributions to Pacific Arctic spring melt onset. Monthly heat flux data [in terawatts (TW)] are gathered from the A3 mooring located at 66.33°N, 168.96°W just north of the Bering Strait on the southern edge of the Chukchi Sea (Woodgate et al. 2015; Woodgate 2018). This mooring is one of an array proximate to the Bering Strait that are funded by the U.S. National Science Foundation-Arctic Observing Network program to monitor characteristics such as volume, salinity, and heat flux of local

Table 1 Range, mean (μ), and standard deviation (σ) of early, late, and average melt onset (MO) cases over the 1979–2015 record

Region	Early MO Range (n = 9)	Early MOμ	Early $MO_σ$	Late range (n = 9)	Late Mμ	Late $MO_σ$	Average MO Range (n = 19)	Average MOμ	Average $MO_σ$
Chukchi Sea	141.12–152.39 May 21–June 1	148.47 May 28	3.99	163.35–167.80 June 12–17	165.11 June 14	1.46	152.76–163.08 June 2–12	157.11 June 6	3.26
Beaufort Sea	146.26–154.77 May 26–June 4	150.92 May 31	3.28	166.03–174.73 June 15–24	168.60 June 18	2.83	155.24–165.88 June 4–15	160.94 June 10	3.03

The Julian day and corresponding date for non-leap years (rounded to the nearest whole day) are additionally shown. Early, late, and average years (n) are listed in Table 2

waters (Serreze et al. 2016a). Heat flux values, calculated with respect to the approximate − 1.9 °C salinity-adjusted freezing point of Bering Strait waters (Steele et al. 2004), represent the amount of heat lost from waters traversing the Bering-Chukchi interchange which could contribute to interannual initiation of seasonal ice melt. Moored heat flux data at the A3 location does not exist prior to September of 1990. We elect to utilize available springtime data thereafter and construct intermittent March – June monthly time series spanning 1991–1992 and 1998–2015 (June 1999 is missing).

In addition to local heat flux observations, North Pacific Ocean surface temperature conditions are analyzed to assess the role of the large-scale thermodynamic environment on melt onset timing characteristics. A commonly used Pacific Decadal Oscillation (PDO; Mantua et al. 1997) index is applied, which represents the first principal component of monthly sea surface temperature anomalies from 20 to 90°N; while the monthly index extends from 1900, we constrain analyses from March to June during the modern melt onset record of 1979–2015.

3 Methodology

To resolve the underlying atmospheric circulation patterns that precondition the Pacific Arctic sea ice cover for melt out, a non-linear, artificial neural network approach, termed the self-organizing map (SOM) (Kohonen 2001), is applied to classify daily ERA-I MSLP conditions within the region. The SOM classification incorporates daily MSLP spatial anomalies, where the daily domain-averaged grid values are subtracted from the raw MSLP at each grid point to isolate the pressure gradients that describe the strength of the near-surface flow across the sea ice. Similar to various other clustering methodologies (e.g. hierarchical, k-means, Ward's), SOMs identify common patterns, or nodes, within a large spatiotemporal, gridded dataset. In reference to this study, the automated, unsupervised SOM procedure iteratively partitions each daily MSLP field into one of a relatively small number of discrete archetypal synoptic patterns. The aim of the SOM is to characterize the range of MSLP circulation in the region by minimizing within pattern variability, while maximizing variability between patterns (Yarnal 1993; Lee and Sheridan 2015). One of the main benefits of SOM-based classification is the ease of visualization of the resulting synoptic climatology of the region, as the procedure maps extreme data values in the corners of the SOM matrix while displaying a gradual transition of similar synoptic states from one node to the next (e.g. Schuenemann et al. 2009; Reusch 2010; Cassano et al. 2015).

As a first step in our classification of the MSLP fields, a principal components analysis is computed for the anomalous MSLP dataset, reducing the initial 3666 grid points of MSLP data into a set of 46 retained principal components (PCs; those with eigenvalues > 1) that account for over 99.3% of the dataset variance. These 46 PCs are used as input into the SOM algorithm in MATLAB's Neural Network Toolbox; thus, the SOM highlights major modes of variability in the principal components of the original dataset, rather than the original data itself. Multiple sizes of SOM dimensions are evaluated, with a 5 × 4 SOM ultimately generated (Fig. 3) after examining multiple internal cluster validation metrics (Calinski-Harabasz Index, Davies-Bouldin Index, Silhouette Index, and the Distributed Variability Skill Score from Lee 2016), externally examining pattern associations with melt onset dates, and based-upon the dimensions used in previous research on Arctic sea ice-atmosphere interactions (Lynch et al. 2016). Through 10,000 iterations, the initial learning rate of 0.90 is decreased to 0.02. The topology is set to "gridtop" (rectangular-shaped), and the distance function is set to "linkdist" (indicating square links and not diagonals). The initial neighborhood radius is 7, and corresponds to the maximum distance (i.e. number of node-to-node steps) between the two most distant SOM nodes, which is based upon the dimensions and distance function. As exhibited by the resulting Sammon map (Supplementary Fig. S1a), the 5 × 4 SOM spans similar distances across the two primary modes of variability (PC1 and PC2), representative of the nearly equal amount of variability explained by these two PCs (28% and 24%, respectively) and warranting a SOM with a nearly equal number of nodes along the two dimensions. When viewed in 3-dimensions (Supplementary Fig. S1b), the SOM takes on a 'saddle-shape' due to the SOM's

ability to capture variability in the third dimension (herein, that is along the 3rd principal component of the dataset due to the antecedent PCA), which accounts for approximately 15% of the variability in the dataset.

After conducting the SOM MSLP anomaly classification, daily V_{10} winds are mapped to each SOM node such that each wind map represents a composite of all days in which a particular MSLP pattern occurs (Fig. 4). We subsequently examined each node's V_{10} wind directions over the Beaufort (B) and Chukchi (C) marginal sea regions and created directional bins for ease of interpretation and to increase the sample size in subsequent frequency composites (more details described below). Aggregations follow onshore (BON/CON), offshore (BOFF/COFF), and along-shore/zonal and weak (BWZ/CWZ), low-level wind direction characteristics proximate to the respective Beaufort Sea and Chukchi Sea coastlines (see Fig. 4). In the event that near-surface winds are multi-directional across a marginal sea (i.e. pattern 9 with easterly flow at Utqiagvik, formerly Barrow, and northerly flow in the Eastern Beaufort) we categorize the pattern's flow according to its winds at Utqiagvik, Alaska which is the approximate coastal locale from which a hydrographic boundary can be drawn separating the eastern edge of the Chukchi Sea from the westernmost flank of the Beaufort Sea.

Given the subseasonal focus of the study, we stratify the directionally-binned frequencies over discrete, sequential 15-day bins (i.e. 1–15, 16–30…61–75) preceding each melt onset date to further resolve the role of short-term, near-surface wind preconditioning effects on ensuing melt. The results are then composited by extrema and average melt onset dates. The 9 earliest and latest melt onsets for each marginal sea are selected as they represent the approximate upper and lowermost quartile of study period (n = 37 years) and are near $\pm 1\sigma$ from the 1981–2010 mean, while the remaining 19 years are characterized as "average" with respect to annual melt dates (Table 2). Late, early, and average year composites are also generated from linearly detrended data series (not shown). Similar extrema are resolved in ~ 50% of late and early cases and exhibit comparable wind frequencies across several intervals (e.g. Chukchi offshore and onshore wind occurrences 46–60 days before early or average melt are within 1d using data with or without trend). These results suggest that by not removing the trend the interannual variability is preserved and the composite analyses are therefore robust to the method selected.

Composite analyses described herein focus on frequency and duration of pattern occurrence within the subseasonal timeframe preceding melt. A Student's two-tailed *t* test is applied to assess whether the deviation in pattern frequencies between extreme cases or extreme versus climatological cases is significant with a null hypothesis of no difference that is rejected at the 95% confidence limit when $p \leq 0.05$. Given that a preponderance of average and early ice melt years occurs over the shorter A3 mooring record, we elect to composite the Bering heat flux data by marginal sea ice melt conditions over available March – June months from 1991 to 2015.

A Mann–Kendall non-parametric trend test (Mann 1945; Kendall 1970) is also utilized to estimate monotonic change signals within the melt onset and aggregated SOM-based frequency and duration time series. This method is chosen over a more common trend analysis approach, such as least-squares regression, to avoid confounding skew-related problems associated with non-normally distributed data series (Smith 2000) and because statistical significance (i.e. the p-value) derived from this test is not heavily weighted by outliers that influence trend magnitude (Dutrieux et al. 2012).

4 Results

4.1 Overview of the SOM patterns and associated synoptic settings

The master 5 × 4 MSLP SOM along with pattern frequencies, representing a percentage monthly occurrence relative to the spring total (100%), are shown in Fig. 3. Positive

Table 2 List of early, late, and average melt onset years (for aggregated SOM frequency and duration analyses) in the Beaufort and Chukchi Seas

Region	Early	Late	Average
Chukchi Sea	1994, **1995**, 1996, **1997**, 2002, **2009**, 2011, **2012, 2014**	1979, **1980**, 1982, **1983, 1984, 1987**, 1988, **2000, 2001**	1981, **1985**, 1986, **1989, 1990**, **1991, 1992**, **1993**, **1998, 1999**, 2003, 2004, **2005**, 2006, **2007**, 2008, **2010**, **2013**, 2015
Beaufort Sea	**1995, 1997**, 2004, 2006, 2008, **2009, 2012, 2014**, 2015	**1980**, 1981, 1983, **1984**, 1986, **1987**, 1994, **2000, 2001**	1979, 1982, **1985**, 1988, **1989, 1990**, **1991, 1992**, **1993**, 1996, **1998, 1999**, 2002, 2003, **2005, 2007, 2010**, 2011, **2013**

Years similarly categorized in both seas are shown in bold. Years with March–June data comprising the A3 mooring composites are underlined (note that monthly A3 data does not exist in June 1999)

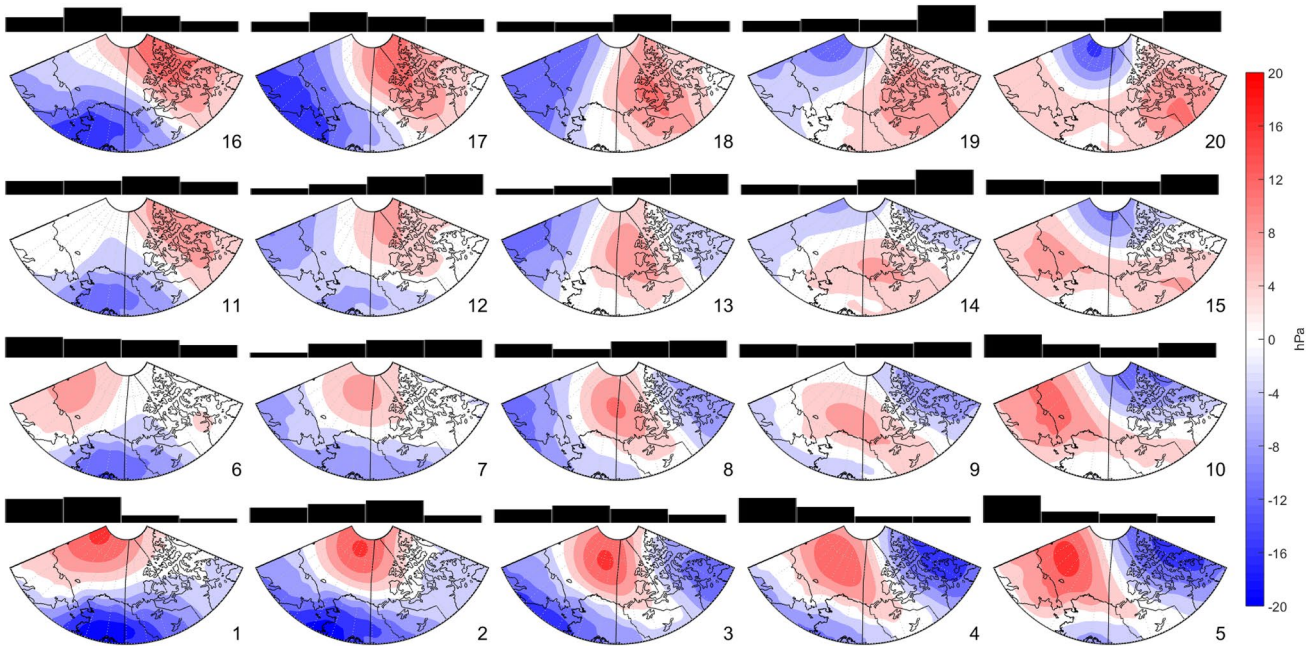

Fig. 3 Master SOM of MSLP anomalies (in hPa) with monthly mean percentage of pattern occurrence from March through June, 1979–2015, shown sequentially from left to right by the height of each bar. For reference, pattern 5 occurs during 9.6% of March days (leftmost bar), and is the most frequently occurring pattern in a given month

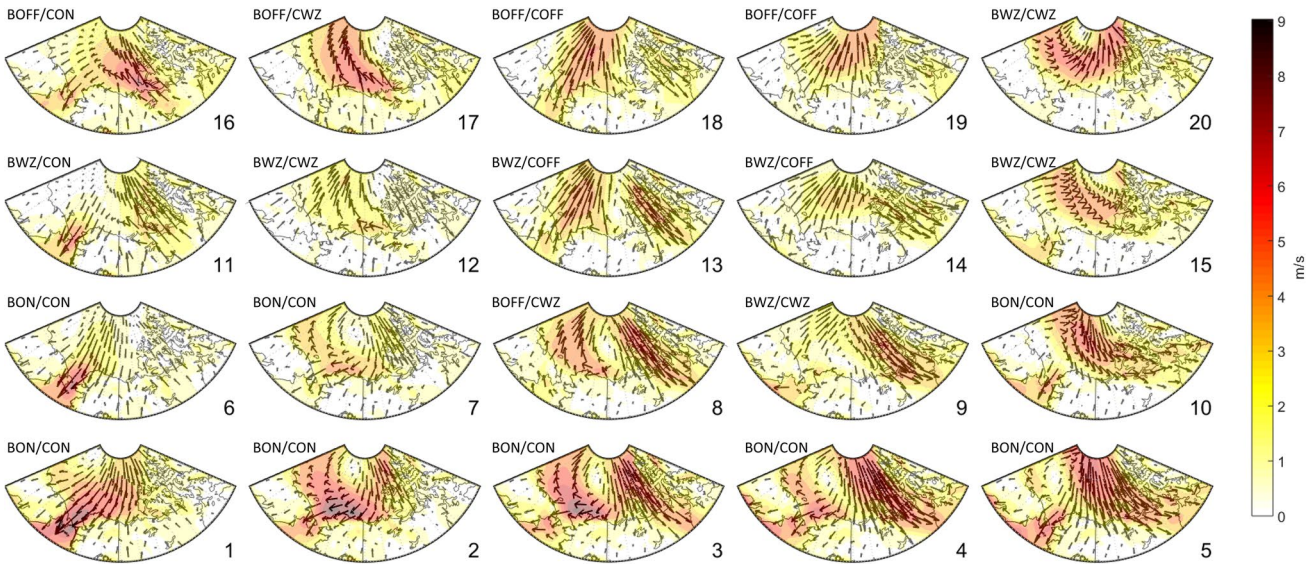

Fig. 4 Composite map of V_{10} winds (in m/s) for days characterized as a particular SOM node in Fig. 3. Based on the vector properties across the Beaufort (B) and Chukchi (C) Seas, each map is classified as onshore (ON), offshore (OFF), or weak/zonal (WZ)

(high) pressure anomalies over the Canadian Archipelago (CA) and eastern Beaufort Sea with negative pressure anomalies over portions of the Chukchi Sea are present across the top row in patterns 16–20. In the bottom row of the matrix, strong and positive pressure anomalies are located over the Beaufort/Chukchi border and extend westward into the East Siberian Sea with negative anomalies predominantly to the south (patterns 1 and 2), east (pattern 5), or both (patterns 3 and 4). Frequency plots characterize the Arctic basin transition from stronger pressure gradients to weaker fields as boreal spring progresses and air temperatures horizontally warm toward the pole.

Pressure gradient strength and inferred low-level circulation from the MSLP SOM is corroborated by V_{10} composites

for days categorized as a particular SOM node (Fig. 4). For example, the strongest magnitude offshore flows (southerly winds) over the Beaufort Sea, as in pattern 17, occur within a gradient of roughly 10–15 hPa. Onshore flows evident in patterns 1–3 exhibit a comparatively similar spatial gradient, albeit with a westward shifted positive pressure anomaly, as prevailing northerly winds of ~6–8 m s^{-1} transport cold Central Arctic air toward the northeastern Siberian and Alaskan Arctic coastlines.

Polar jet stream ridging in the 500 hPa GPH field coincides with the presence of surface high pressure anomalies found typically downstream of the ridge axis as in Fig. 5. A ridge near the Beaufort-Chukchi maritime boundary is found in pattern 8 supporting offshore flows; a similar feature is evident in pattern 13, though is shifted southeastward over the eastern Beaufort Sea supporting more alongshore surface winds. Closed anticyclones near the northwestern edge of the domain (e.g. patterns 1–5) promote widespread onshore flow and cold air advection off the ice-covered Central Arctic Ocean surface. Spatial variations in the 925 hPa air temperature composites tend to follow the path of geostrophic low-level winds and upper-air circulation (Fig. 6). For example, patterns 18 and 19 correspond with southerly/southwesterly flow across Bering Strait and low elevation Chukotka and Arctic Alaska coastal areas. These winds support incursions of above-freezing air near the land-seasonal ice interface at the coast where onset of break-up tends to originate (Fig. 6). Onshore flow examples with prevailing sub-freezing flow tend to penetrate this coastal boundary, with cold surges extending inland several hundred kilometers (patterns 4 and 5).

4.2 Melt onset and the role of circulation frequency and duration

Downward trends indicating earlier melt onset are apparent features within the Beaufort and Chukchi Sea time series (Fig. 2). Early, late, and average melt cases are relatively coherent between the respective marginal seas with dates falling within 5 days of each other (Table 1). Open water tends to develop earlier in the Chukchi versus the Beaufort due to the former sea's relative southerly extent and interactions with Pacific water and air masses. Despite these differences due to geography and regional oceanography, the Beaufort long-term melt trend is slightly stronger (-0.42 days $year^{-1}$) than that of the Chukchi (-0.34 days $year^{-1}$) with both trends significant at the nominal $p \leq 0.05$ level. A consistent clustering of melt dates near 1 June becomes common from 2004 with late extremes not observed after 2001 with respect to the long-term record (Fig. 2; Table 1). In contrast, the previous decades of the melt onset record are marked by greater interannual variability (expressed in 7-year running standard deviations, not shown) with melt observed from late-May to late-June. Trends calculated here through 2015 and extrapolated to the decadal scale are slightly accelerated from Stroeve et al. (2014), which conclude in 2013 and use least squares regression. Unlike clear melt signals in the sea ice time series, temporal trends calculated for the SOM pattern frequencies and duration bins (discussed through this section) are not significant (not shown), indicating that earlier melt is not the result of underlying monotonic tendencies in the precursor atmospheric conditions.

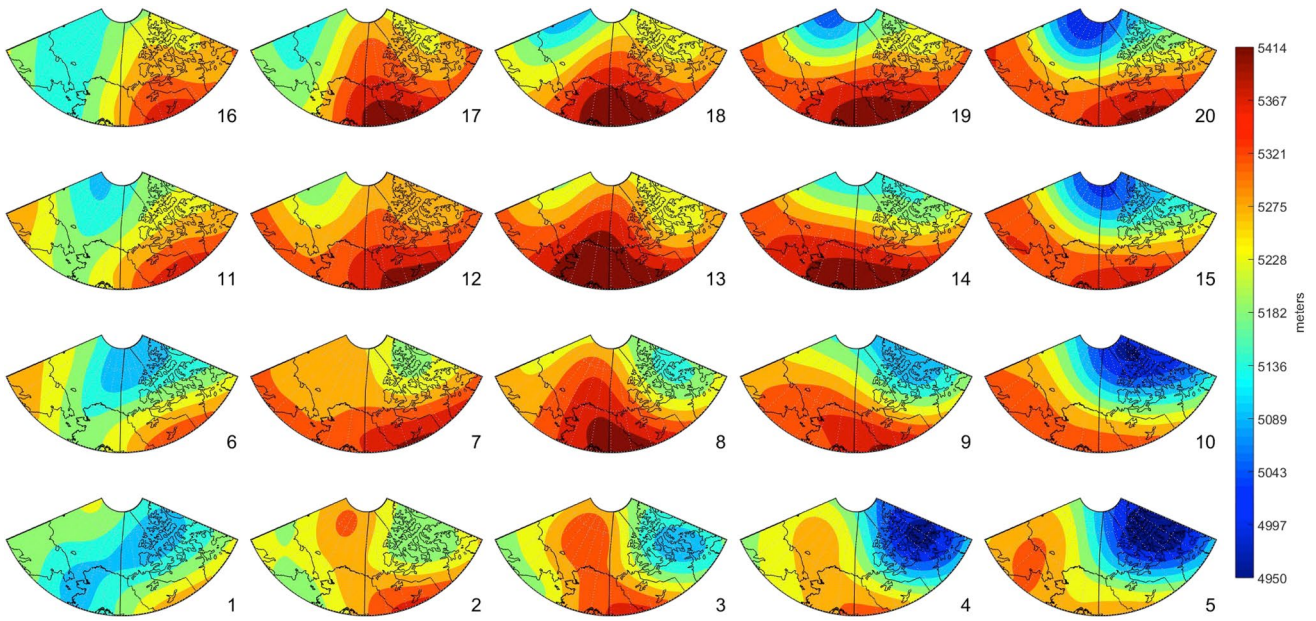

Fig. 5 Composite 500 hPa GPH values (in meters) for all days classified as one of 20 SOM patterns

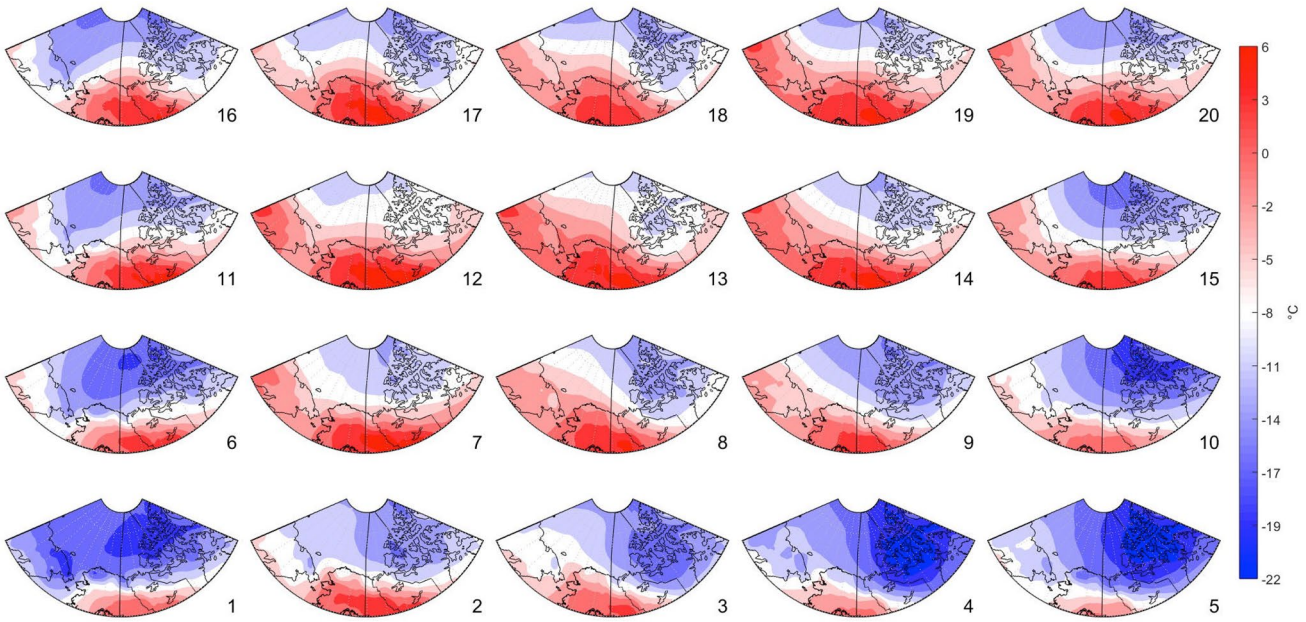

Fig. 6 Composite 925 hPa air temperatures (in ºC) for all days characterized as one of 20 SOM patterns

The occurrence of geostrophic flow patterns, aligned with the surface pressure SOM and associated V_{10} winds, across each marginal sea are initially assessed in a cumulative fashion over the 75-days leading up to melt onset (Supplementary Fig. S2). Roughly 40–50% of days preceding average melt are characterized by northerly winds, but a slight reduction in their occurrence is observed in both seas during early melt onset cases. Over this period, zonal flow occurs ~ 1–4 days more often across the Beaufort and Chukchi in early years than average or late years, while there are 2–4 fewer days of onshore, northerly prevailing winds during early melt versus late melt cases (Supplementary Fig. S2).

To further isolate the role of intraseasonal synoptic forcing associated with melt anomalies, we elected to bin the pattern frequencies in sequential 15-day increments. In the Beaufort Sea (Fig. 7a–j), onshore flow occurrence diminishes through late winter and spring giving way to more zonal and offshore flow. This interseasonal difference in the wind direction could explain why ~ 3 fewer onshore days ($p < 0.05$) occur in the 1–15 day period during late minus average years. The increased incidence of offshore (southerly component) winds partially compensates for fewer onshore patterns (Fig. 7a, b). A similar reduction of onshore flow regimes characterizes the 31–45 days preceding early melt years with increased frequency of offshore and zonal winds alongshore. In contrast, at 61–75 days preceding melt, northerly wind incidence becomes more common with late and early melt onsets. Frigid air from the Central Arctic Ocean is advected south by the prevailing northerlies leading to Beaufort and Chukchi 925 hPa air temperature anomalies between − 2 and − 4 °C in cold and warm seasons (Serreze et al. 2011); these events are more common when the ice melts later than average. Days characterized by zonal winds are significantly reduced in this period (by ~ 2 days) to compensate for increased northerly flow and transport of Arctic air masses off the thicker, multiyear ice around the North Pole (Fig. 7i, j).

Differences in onshore pattern occurrence between the early and late melt years in the Chukchi region are apparent in the discrete 16–30, 31–45, 46–60, and 61–75 day windows with 2–3 day reductions of northerly flow (Fig. 8d, f, h, j). Within the 46–60 day window preceding early melt onset cases, these wind regimes tend to occur significantly ($p < 0.05$) less often, ~ 3.5 days versus average years, offset by increased incidence (~ 2.5 days) of zonal flow that is similarly significant (Fig. 8g, h). Distinct periods of anomalous southerly, offshore wind patterns tend to occur more frequently in early melt cases as onshore winds and cold advection are comparatively limited.

To gain perspective on the role of near-surface windflow persistence as a preconditioning factor to melt onset, we assess events lasting 3–4, 5–6, and 7 + consecutive days within the 75 days before melt transpires (Supplementary Fig. S3a–f). In the Beaufort Sea, zonal wind events of 3–4 days duration are slightly more common (+ 1 event) in early versus average and late melt years (Supplementary Fig. S3b). In contrast, during late melt years the persistent offshore events are found to decrease around 1 event relative

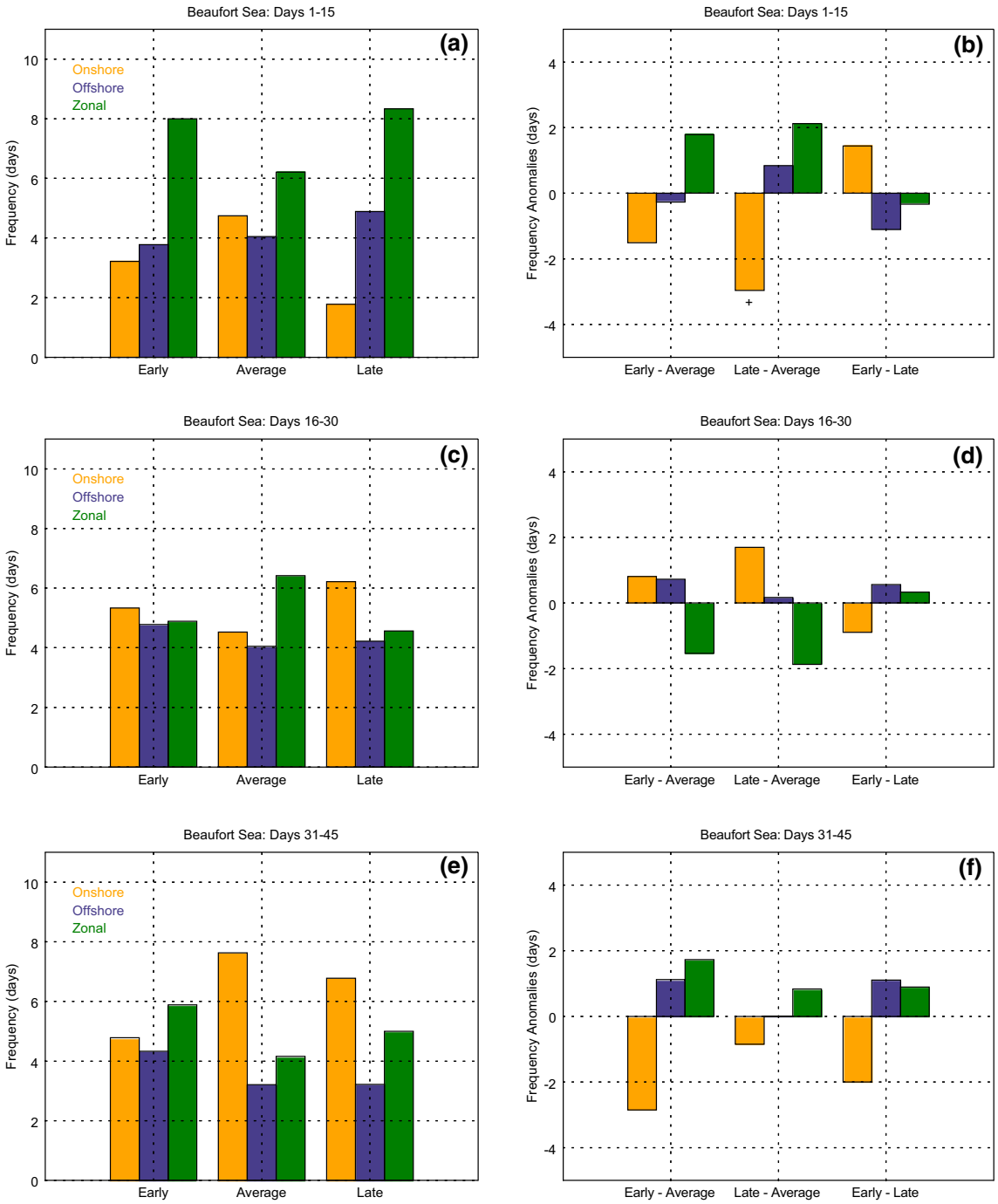

Fig. 7 Composite frequencies of onshore, offshore, and zonal patterns and their differences for Beaufort early, average and late melt cases in the 1–15 (**a, b**), 16–30 (**c, d**), 31–45 (**e, f**), 46–60 (**g, h**), and 61–75 (**i, j**) days preceding melt. Statistically significant differences ($p \leq 0.05$) are indicated by a plus sign (+) near the bars

to average and early melt incidence. Little change, less than 1 event, is noted in the other persistence bins.

The duration of a directional wind regime appears to have a stronger link to Chukchi Sea melt than in the adjacent Beaufort region. Onshore flow events of 3–4 days are common across Chukchi waters (> 8 events per 75-day period, hereafter "period") regardless of melt category (Supplementary Fig. S4a). Differences in offshore flow events are notable, however, as 2 more persistent events of southerly component winds tend to occur with early versus to late onset years (Supplementary Fig. S4b). Long-term dynamic persistence (≥7 days) plays a role in melt also through

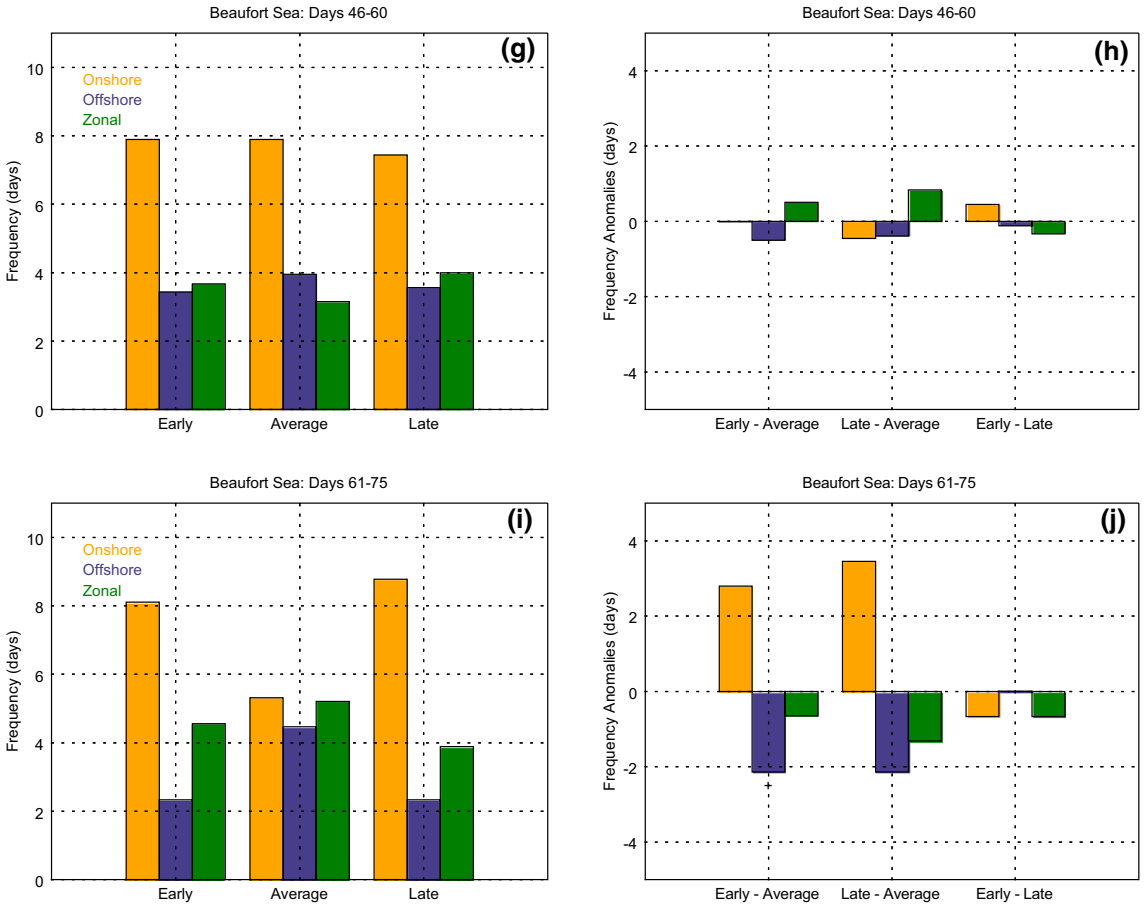

Fig. 7 (continued)

reductions in onshore patterns of ~2 events period^{-1} in early versus average cases and ~1.5 events period^{-1} in early and late differences. Slight increases in short-term offshore flow (3–4 days) paired with fewer onshore events lasting at least one week appear to precondition the ice for early melt out.

4.3 Bering inflow and the North Pacific thermodynamic state

Low-level winds tend to advect relatively mild air from the North Pacific or snow-free Arctic lands, or transport frigid air off the Central Arctic Ocean onto the Beaufort and Chukchi ice cover. The occurrence and persistence of such wind patterns are shown to have a subseasonal preconditioning effect on the timing of sea ice break-up events and commencement of the melt season. However, also important to ice melt and break-up is the thermodynamic environment of the North Pacific Ocean. Variations in the heat content at both the local and regional scale modulate the impact of variations in the concurrent wind regimes. To provide insight on the role of ocean forcing on melt onset, an analogous composite framework is applied to the North Pacific Ocean through monthly-averaged (1) PDO index values and (2) moored heat flux data from the A3 Bering site.

Complementary analyses to Sects. 4.1 and 4.2 are conducted for overlapping periods in the A3 and PDO record for the Beaufort and Chukchi marginal seas (Tables 2, 3). For the Beaufort Sea, early melt onset years are characterized by weakly positive March–June PDO values. In late melt cases, PDO values are consistently $\geq 1\sigma$ in climatological spring (MAM), while March and April exhibit significantly greater values in late versus average years and significantly reduced values in early versus late years (Table 3a). Higher heat flux values in March, May, and June are also characteristic of late versus early melting across the area (Table 3b). Though June heat flux values are significantly higher in late relative to early years, the small sample (n = 2) should preclude overconfidence in a strong linkage. In late Beaufort melt years, recall that the subseasonal distribution of winds is such that onshore flow is favored to offshore winds (Supplementary Fig. S2), with more frequent northerly winds as the intervals regress from the 16–30 to 61–75-day periods preceding melt (Fig. 7c–f). The prevailing northerlies may therefore suppress positive PDO warm air incursions, emanating from the

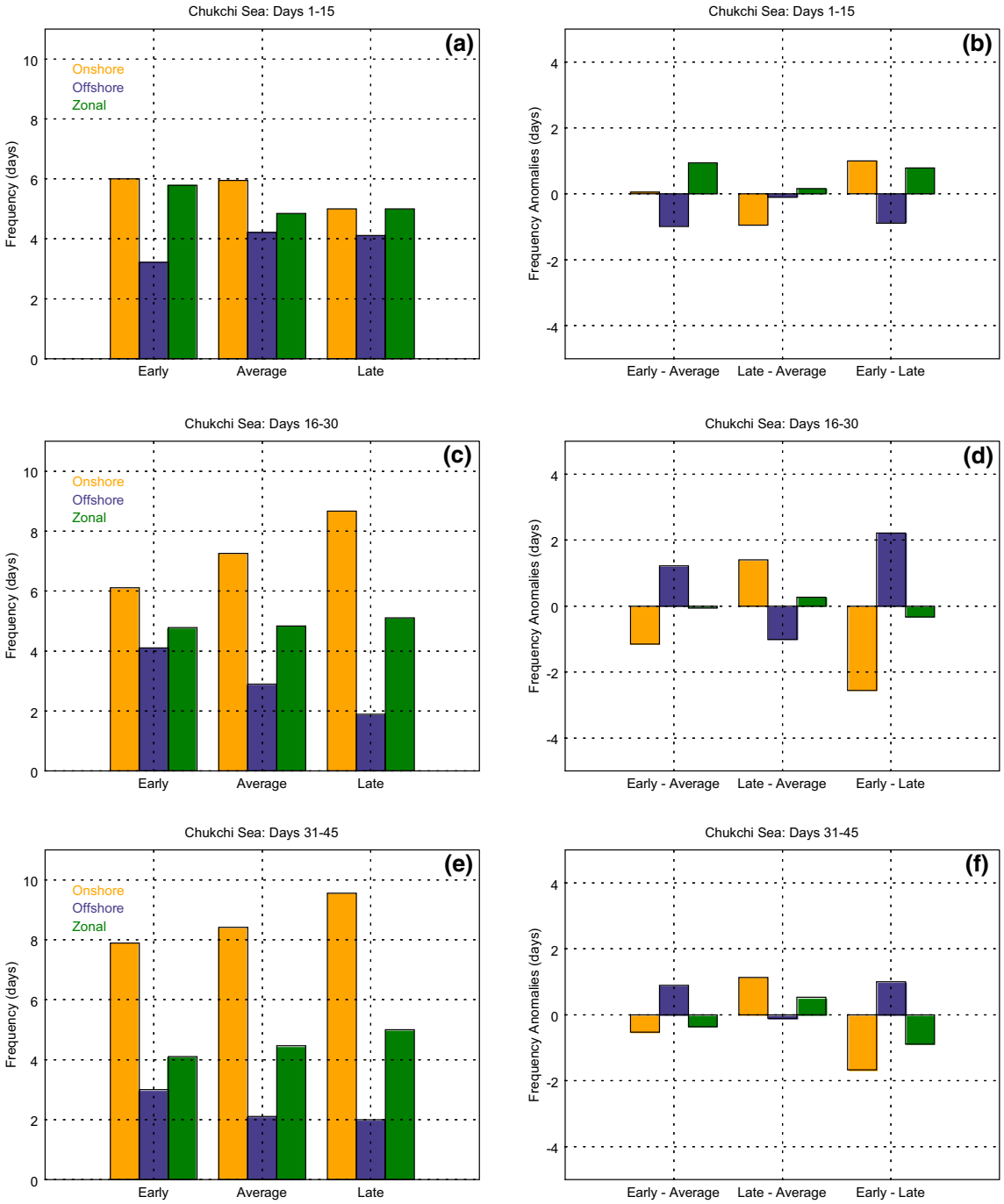

Fig. 8 Composite frequencies of onshore, offshore, and zonal patterns and their differences for Chukchi early, average and late melt cases in the 1–15 (**a, b**), 16–30 (**c, d**), 31–45 (**e, f**), 46–60 (**g, h**), and 61–75 (**i, j**) days preceding melt. Statistically significant differences ($p \leq 0.05$) are indicated by a plus sign (+) near the bars

Gulf of Alaska, across maritime northern Alaska and steer heat inflow away from the Beaufort region.

Whereas positive heat flux anomalies do not appear to have a demonstrable effect on early melt of the seasonal Beaufort Sea ice cover, ocean heat anomalies and synoptic winds appear to couple to reinforce Chukchi melt timing. Early melt events in the Chukchi Sea are similarly characterized by slightly positive monthly PDO values ($\leq 0.60\sigma$) in March–June, while late ice break-up is characterized by comparatively higher index values of at least 0.83σ in March, April, and May (Table 3c). March PDO index values are significantly negative (-1.03σ) in early versus late

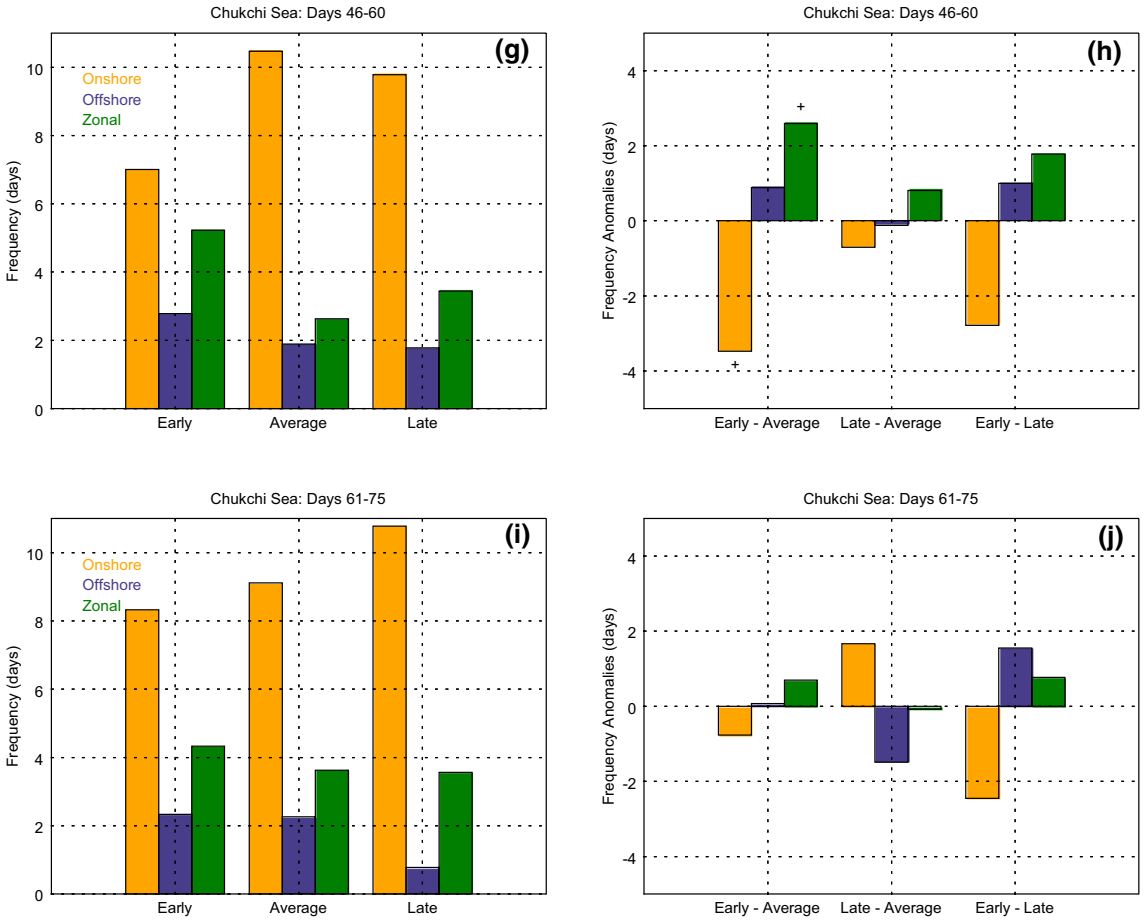

Fig. 8 (continued)

years. Composite heat flux values are higher in all months when seasonal ice melt occurs early versus late, especially in May and June (Table 3d). Early Chukchi melt years coincide with diminished northerlies and increased southerly flow over the 16–75 days before melt with additional increased zonal flow occurrences at the early half of the subseasonal period (46–75 days) to propagate the transport of ocean heat into Chukchi waters (Fig. 8c–j).

5 Summary and discussion

Recent studies have identified monthly-to-seasonally averaged ocean–atmosphere contributions to Pacific Arctic extreme melt cases and decadal-to-multidecadal patterns in open water development (e.g. Kwok et al. 2013; Frey et al. 2015; Serreze et al. 2016a). However, considerably less attention has been focused toward identifying the incidence of atmospheric regimes, namely wind patterns, within a seasonal timeframe preceding ice melt and break-up anomalies (e.g. Drobot et al. 2009). Such a knowledge gap in a rapidly changing region of the Arctic motivates this investigation, which applies the SOM technique to quantify the frequency and duration of surface pressure patterns that precondition the Beaufort and Chukchi ice cover for melt onset and subsequent loss (from additional melt and ice advection) through the melt season.

The location of synoptic surface pressure patterns over the Beaufort and Chukchi Seas, including the positioning of the Beaufort High, are shown to influence the low-level wind pattern frequencies and resulting ice melt timing. Zonal flow, manifest primarily as weak easterly winds along the Alaskan coast, tends to increase over the 75 days preceding Beaufort and Chukchi early melt years (~ 2 and 4 days versus average, respectively). This finding reflects a tendency for anticyclones to traverse eastward from the northwest or central Chukchi toward the Beaufort Sea, perhaps preferentially to early break-up areas (Steele et al. 2015). Within the discrete time windows before early Beaufort melt, ~ 1–2 more zonal and/or offshore flow days occur within each 15-day period out to 61–75 days, offset by similar magnitude reductions in the onshore winds, especially at 1–15 and 31–45 day periods. Similarly (as early melt years overlap between seas in 5 of 9 cases), the

Table 3 Composite values of the normalized PDO index and A3 mooring heat flux (in terawatts (TW)) for the respective records indicated in Table 2

	March	April	May	June
(a) Beaufort: PDO				
Early	0.19	0.22	0.46	0.55
Average	0.30	0.38	0.54	0.18
Late	1.31	1.24	1.10	0.58
Early-Average	−0.11	−0.16	−0.08	0.37
Late-Average	**1.01**	**0.85**	0.56	0.40
Early-Late	**−1.12**	**−1.02**	−0.64	−0.03
(b) Beaufort: A3 (in TW)				
Early (n = 7)	0.30	0.49	3.37	11.10
Average (n = 11)	0.37	0.41	2.52	13.22
Late (n = 2)	0.55	0.35	4.00	21.60
Early-Average	−0.07	0.08	0.85	−2.12
Late-Average	0.18	−0.06	1.48	8.38
Early-Late	−0.25	0.14	−0.63	**−10.50**
(c) Chukchi: PDO				
Early	0.05	0.32	0.60	0.47
Average	0.47	0.46	0.61	0.37
Late	1.08	0.97	0.83	0.25
Early-Average	−0.42	−0.15	−0.01	0.10
Late-Average	0.61	0.50	0.23	−0.12
Early-Late	**−1.03**	−0.65	−0.24	0.21
(d) Chukchi: A3 (in TW)				
Early (n = 5)	0.40	0.50	3.00	12.66
Average (n = 13)	0.32	0.42	2.79	12.22
Late (n = 2)	0.15	0.20	1.25	6.35
Early-Average	0.08	0.08	0.21	0.44
Late-Average	−0.17	−0.22	−1.54	−5.87
Early-Late	0.25	0.30	1.75	6.31

Sample sizes (n) at the A3 site are indicated due to the record's abbreviated nature. Statistically significant differences ($p \leq 0.05$) are shown in bold type

eastward shift in anticyclonic activity toward the Beaufort during early Chukchi melt occurrences coincides with decreased northerlies and increased zonal and/or offshore flow by 1–3 days.

The intensity and direction of the flow are also modulated by tandem cyclonic positioning and strength (i.e. gradient associated with negative pressure anomalies). High pressure values extending eastward from the Beaufort Sea toward Greenland with low pressure over Siberia and adjacent waters are characteristic of the late spring/early summer (May–June) Arctic surface pressure field since 2007 (Overland et al. 2012a, 2018). The development of this pressure dipole mechanism during recent spring months may be responsible for the decreased (increased) frequency and duration of northerly (southerly) meridional winds, thereby preconditioning the Pacific Arctic ice cover for either climatologically average (in colder years) or early melt occurrence since the early-2000s.

In conjunction with previous work at coarser temporal scales (e.g. MAM), the location, intensity, and persistence of the Beaufort High is shown to influence the Pacific Arctic warm season climate and cryosphere. A strong anticyclone about the region tends to favor positive near-surface springtime air temperatures through solar heating of the ice pack (Serreze and Barrett 2011; their Fig. 14). Though Serreze and Barrett (2011) did not find trends in seasonal occurrence of anticyclonic winds over the 1979–2008 climatology, Ballinger et al. (2014) used a clustering approach and found that the frequency of Beaufort High patterns (days characterized by positive pressure anomalies) in the March–September melt season had increased by nearly 20 days from 1979 to 2006 to the 2007–2012 period alone. Of note, the change in the latter period represents an accelerated increase in Beaufort High days from the 1979–1995 mean (Ballinger et al. 2014). Higher Pacific Arctic surface pressures may reflect a concurrent expansion of the 500 hPa GPH field over Alaska (McLeod et al. 2018). Two recent decades of increased anticyclonic activity about the region have thus enhanced downward shortwave radiation and easterly wind contributions to earlier melt onset and polynya expansion (Moore and Pickart 2012; Wood et al. 2015), and influenced heat advection off the snow-free North Slope land which tends to melt out roughly one week before the adjacent seasonal ice cover (Cox et al. 2017).

The regional wind field is also shown to play a role modulating the North Pacific climate influence on melt onset. Late melt onset cases (also congruent by sea in 6 of 9 years) coincide with a greater frequency of onshore flow across the Chukchi and Beaufort. These northerlies may inhibit positive PDO-associated southerly warm air advection and above-normal winter and spring air temperatures from extending beyond the North Slope and into west Arctic maritime areas (Table 3; Walsh et al. 2017; Wang et al. 2017, 2018). By comparison, lower though slightly positive composite PDO values in early melt years coincide with greater incidence of easterly and southerly winds in the Pacific Arctic with fewer northerlies. A thinner areal pack comprising increasing amounts of first-year ice (formed during the prior autumn–winter freeze period) also renders the ice sensitive to (thermo)dynamic drivers of early melt (Tooth and Tschudi 2018). The Aleutian Low (AL) also is known to exhibit episodic intradecadal variation relative to low-frequency PDO phases and tends to increase warm air advection into the Arctic when shifted northwestward from its climatological mean position to the western Aleutian chain (Overland et al. 2012b; Newman et al. 2016). AL intensification coupled with a westward progression may thus enhance North Pacific pressure gradient forcing and heat flux transport through the Bering Strait and into the

Chukchi and Beaufort Seas by local hydrography (Woodgate 2018). With the stochastic nature of weather patterns, namely interseasonal cyclogenesis variability in the North Pacific, we hypothesize that such sea surface temperature and AL coupling could vary substantially within past early or late melt onset years, and such speculation warrants further investigation.

Future projections derived from fifth phase of the Coupled Model Intercomparison Project (CMIP5) suggest a ~3–5 week annual lengthening of Pacific Arctic ice-free conditions during the 2015–2044 period assuming an RCP8.5 unabated emissions scenario (Wang et al. 2018). Given the likelihood that the region's melt season will continue to lengthen, continued monitoring of the frequency and duration of atmospheric circulation regimes will be important to understand the evolution of sea ice melt and break-up patterns in response to winter and spring wind characteristics. Ongoing oceanographic monitoring programs that capture high temporal resolution data streams at the tails of the melt season, such as the Arctic Heat Open Science Experiment (Wood et al. 2018), will continue to provide observational insights into the coupled ocean–atmosphere environment driving seasonal ice melt with emanating benefits to sea-ice forecasting.

Acknowledgements We thank the Editor and anonymous reviewers for constructive comments on the manuscript. We thank Jeffrey Miller for updating the melt onset time series, and data are available at https://neptune.gsfc.nasa.gov/csb/index.php?section=54. ERA-I data fields come from European Center for Medium Range Forecasting (https://www.ecmwf.int/en/forecasts/datasets/reanalysis-datasets/era-interim) and PDO index values and additional details may be found at http://research.jisao.washington.edu/pdo/. Bering Strait heat flux data are obtained from psc.apl.washington.edu/BeringStrait.html and we thank Rebecca Woodgate for making the time series available. We also thank William Plunket and Saeideh Gharehchahi for assistance with data analysis. TJB acknowledges support from Texas State University's Research Enhancement Program. This is PMEL contribution number 4749. This publication is partially funded by the Joint Institute for the Study of the Atmosphere and Ocean (JISAO) under NOAA Cooperative Agreement NA15OAR4320063, Contribution No. 2018-0137.

References

Amante C, Eakins BW (2009) ETOPO1 1 Arc-Minute Global Relief Model: procedures, data sources and analysis (no. 24). NOAA technical memorandum NESDIS NGDC. https://www.ngdc.noaa.gov/mgg/global/global.html

Ballinger TJ, Rogers JC (2014) Climatic and atmospheric teleconnection indices and western Arctic sea ice variability. Phys Geog 35:459–477. https://doi.org/10.1080/02723646.2014.949338

Ballinger TJ, Sheridan SC (2014) Associations between circulation pattern frequencies and sea ice minima in the western Arctic. Int J Climatol 34:1385–1394. https://doi.org/10.1002/joc.3767

Ballinger TJ, Sheridan SC (2015) Regional atmospheric patterns and the delayed sea-ice freeze-up in the western Arctic. Clim Change 131:229–243. https://doi.org/10.1007/s10584-015-1383-5

Ballinger TJ, Schmidlin TW, Steinhoff DF (2013) The polar marine climate revisited. J Clim 26:3935–3952. https://doi.org/10.1175/JCLI-D-12-00660.1

Ballinger TJ, Sheridan SC, Hanna E (2014) Resolving the Beaufort Sea High using synoptic climatological methods. Int J Climatol 34:3312–3319

Cassano EN, Glisan JM, Cassano JJ, Gutowski WJ Jr, Seefeldt MW (2015) Self-organizing map analysis of widespread temperature extremes in Alaska and Canada. Clim Res 62:199–2018. https://doi.org/10.3354/cr01274

Comiso JC, Meier WN, Gersten R (2017) Variability and trends in Arctic Sea ice cover: results from different techniques. J Geophys Res Oceans 122:6883–6900. https://doi.org/10.1002/2-17JC012768

Cox C, Stone R, Douglas D, Stanitski D, Divoky G, Dutton G, Sweeney C, George J, Longenecker D (2017) Drivers and environmental responses to the changing annual snow cycle of northern Alaska. Bull Am Meteorol Soc 98:2559–2577. https://doi.org/10.1175/BAMS-D-16-0201.1

Dee DP, Uppala SM, Simmons AJ, Berrisford P, Poli P, Kobayashi S, Andrae U, Balmaseda MA, Balsamo G, Bauer P, Bechtold P, Beljaars ACM, van de Berg L, Bidlot J, Bormann N, Delsol C, Dragani R, Fuentes M, Geer AJ, Haimberger L, Healy SB, Hersbach H, Hólm EV, Isaksen L, Kållberg P, Köhler M, Matricardi M, McNally AP, Monge-Sanz BM, Morcrette J-J, Park BK, Peubey C, de Rosnay P, Tavolato C, Thépaut J-N, Vitart F (2011) The ERA-Interim reanalysis: configuration and performance of the data assimilation system. Q J R Meteorol Soc 137:553–597. https://doi.org/10.1002/qj.828

Drobot SD, Maslanik JA, Anderson MR (2009) Interannual variations in the opening date of the Prudhoe Bay shipping season: links to atmospheric and surface conditions. Int J Climatol 29:197–203. https://doi.org/10.1002/joc.1725

Dutrieux LP, Bartholomeus H, Herold M, Verbesselt J (2012) Relationships between declining summer sea ice, increasing temperatures and changing vegetation in the Siberian Arctic tundra from MODIS time series (2000–11). Environ Res Lett 7:044028. https://doi.org/10.1088/1748-9326/7/4/044028

Eguíluz VM, Fernández-Gracia J, Irigoien X, Duarte CM (2016) A quantitative assessment of Arctic shipping in 2010–2014. Sci Rep 6:30682. https://doi.org/10.1038/srep30682

Frey KE, Moore GWK, Cooper LW, Grebmeier JM (2015) Divergent patterns of recent sea ice cover across the Bering, Chukchi, and Beaufort seas of the Pacific Arctic Region. Prog Oceanogr 136:32–49

Grebmeier JM, Overland JE, Moore SE, Farley EV, Carmack EC, Cooper LW, Frey KE, Helle JH, McLaughlin FA, McNutt SL (2006) A major ecosystem shift in the northern Bering Sea. Science 311:1461–1464

Kashiwase H, Ohshima KI, Nihashi S, Eicken H (2017) Evidence for ice-ocean albedo feedback in the Arctic Ocean shifting to a seasonal ice zone. Sci Rep 7:8170. https://doi.org/10.1038/s41598-017-08467-z

Kendall MG (1970) Rank correlation methods, 4 edn. Charles Griffin, London, pp 202

Kohonen T (2001) Self-organizing maps, 3 rd edn. Springer, New York, pp 501

Kwok R, Cunningham GF (2010) Contribution of melt in the Beaufort Sea to the decline in Arctic multiyear sea ice coverage: 1993–2009. Geophys Res Lett 37:L20501. https://doi.org/10.1029/2010GL044678

Kwok R, Spreen G, Pang S (2013) Arctic sea ice circulation and drift speed: decadal trends and ocean currents. J Geophys Res Oceans 118:1–18. https://doi.org/10.1002/jgrc.20191

L'Heureux ML, Kumar A, Bell GD, Halpert MS, Higgins RW (2008) Role of the Pacific-North American (PNA) pattern in the 2007

Arctic sea ice decline. Geophys Res Lett 35:L20701. https://doi.org/10.1029/2008GL035205
Lee CC (2016) Reanalyzing the impacts of atmospheric teleconnections on cold-season weather using multivariate surface weather types and self-organizing maps. Int J Climatol 37:3714–3730. https://doi.org/10.1002/joc.4950
Lee CC, Sheridan SC (2015) Synoptic climatology: an overview. Reference module in earth systems and environmental sciences. Elsevier. https://doi.org/10.1016/B978-0-12-409548-9.09421-5
Lindsay R, Wensnahan M, Schweiger A, Zhang J (2014) Evaluation of seven different reanalysis products in the Arctic. J Clim 27:2588–2606. https://doi.org/10.1175/JCLI-D-13-00014.1
Lynch AH, Serreze MC, Cassano EN, Crawford AD, Stroeve J (2016) Linkages between Arctic summer circulation regimes and regional sea ice anomalies. J Geophys Res Atmos 121:7868–7880. https://doi.org/10.1002/2016/JD025164
Mann HB (1945) Non-parametric test against trend. Econometrica 13:245–259
Mantua NJ, Hare SR, Zhang Y, Wallance JM, Francis RC (1997) A Pacific interdecadal climate oscillation with impacts on salmon production. Bull Am Meteorol Soc 78:1069–1079
Markus T, Stroeve JC, Miller J (2009) Recent changes in Arctic sea ice melt onset, freezeup, and melt season length. J Geophys Res 114:C12024. https://doi.org/10.1029/2009JC005436
McLeod JT, Ballinger TJ, Mote TL (2018) Assessing the climatic and environmental impacts of mid-tropospheric anticyclones over Alaska. Int J Climatol 38:351–364. https://doi.org/10.1002/joc.5180
Moore GWK, Pickart RS (2012) The Wrangel Island Polynya in early summer: trends and relationships to other polynyas and the Beaufort Sea High. Geophys Res Lett 39:L05503. https://doi.org/10.1029/2011GL050691
Newman M, Alexander MA, Ault TR, Cobb KM, Deser C, Di Lorenzo E, Mantua NJ, Miller AJ, Minobe S, Nakamura H, Schneider N, Vimont DJ, Phillips AS, Scott JD, Smith CA (2016) The Pacific Decadal Oscillation, revisited. J Clim 29:4399–4427
Nghiem SV, Hall DK, Rigor IG, Li P, Neumann G (2014) Effects of Mackenzie River discharge and bathymetry on sea ice in the Beaufort Sea. Geophys Res Lett 41:873–879. https://doi.org/10.1002/2013GL058956
Overland JE, Francis JA, Hanna E, Wang M (2012a) The recent shift in early summer atmospheric circulation. Geophys Res Lett 39:L19804. https://doi.org/10.1029/2012GL053268
Overland JE, Wang M, Wood KR, Percival DB, Bond NA (2012b) Recent Bering Sea warm and cold events in a 95-year context. Deep-Sea Res II 65–70:6–13. https://doi.org/10.1016/j.dsr2.2012.02.013
Overland JE, Wang M, Ballinger TJ (2018) Recent increased warming of the Alaskan marine Arctic due to midlatitude linkages. Adv Atmos Sci 35:75–84. https://doi.org/10.1007/s00376-017-7026-1
Peng G, Meier WN (2018) Temporal and regional variability of Arctic sea-ice coverage from satellite data. Ann Glaciol 59:191–200. https://doi.org/10.1017/aog.2017.32
Perovich DK, Jones KF, Light B, Eicken H, Markus T, Stroeve J, Lindsay R (2011) Solar partitioning in a changing Arctic sea-ice cover. Ann Glaciol 52:192–196
Petty AA, Tsamados MC, Kurtz NT, Farrell SL, Newman T, Harbeck JP, Feltham DL, Richter-Menge JA (2016) Characterizing Arctic sea ice topography using high-resolution IceBridge data. Cryosphere 10:1161–1179. https://doi.org/10.5194/tc-10-1161-2016
Polyakov IV, Walsh JE, Kwok R (2012) Recent changes of Arctic multiyear sea ice coverage and the likely causes. Bull Am Meteor Soc 93:145–151
Reusch DB (2010) Nonlinear climatology and paleoclimatology: capturing patterns of variability and change with self-organizing maps. Phys Chem Earth 35:329–340. https://doi.org/10.1016/j.pce.2009.09.001
Schuenemann KC, Cassano JJ, Finnis J (2009) Synoptic forcing of precipitation over Greenland: climatology for 1961–99. J Hydrometeorol 10:60–78. https://doi.org/10.1175/2008JHM1014.1
Serreze MC, Barrett AP (2011) Characteristics of the Beaufort Sea High. J Clim 24:159–182
Serreze MC, Barrett AP, Cassano JJ (2011) Circulation and surface controls on the lower tropospheric air temperature field of the Arctic. J Geophys Res 116:D07104. https://doi.org/10.1029/2010JD015127
Serreze MC, Crawford AD, Stroeve JC, Barrett AP, Woodgate RA (2016a) Variability, trends, and predictability of seasonal sea ice retreat and advance in the Chukchi Sea. J Geophys Res Oceans 121:7308–7325. https://doi.org/10.1002/2016JC011977
Serreze MC, Stroeve J, Barrett AP, Boisvert LN (2016b) Summer atmospheric circulation anomalies over the Arctic Ocean and their influences on September sea ice extent: a cautionary tale. J Geophys Res Atmos 121(11):463–11485
Simmonds I (2015) Comparing and contrasting the behavior of Arctic and Antarctic sea ice over the 35 year period 1979–2013. Ann Glaciol 56:18–28. https://doi.org/10.3189/2015AoG69A909
Simmonds I, Rudeva I (2012) The great Arctic cyclone of August 2012. Geophys Res Lett 39:L23709. https://doi.org/10.1029/2012GL054259
Smith LC (2000) Trends in Russian Arctic river-ice formation and breakup, 1917 to 1994. Phys Geog 21:46–56
Steele M, Morison J, Ermold W, Rigor I, Ortmeyer M, Shimada K (2004) Circulation of summer Pacific halocline water in the Arctic Ocean. J Geophys Res 109:C02027. https://doi.org/10.1029/2003JC002009
Steele M, Dickinson S, Zhang J, Lindsay R (2015) Seasonal ice loss in the Beaufort Sea: toward synchrony and prediction. J Geophys Res Oceans 120:1118–1132. https://doi.org/10.1002/2014JC010247
Stroeve JC, Markus T, Boisvert L, Miller J, Barrett A (2014) Changes in Arctic melt season and implications for sea ice loss. Geophys Res Lett 41:1216–1225. https://doi.org/10.1002/2013GL058951
Tooth M, Tschudi M (2018) Investigating Arctic sea ice survivability in the Beaufort Sea. Remote Sens 10:267. https://doi.org/10.3390/rs10020267
Walsh JE, Bieniek PA, Brettschneider B, Euskirchen ES, Lader R, Thoman RL (2017) The exceptionally warm winter of 2015-16 in Alaska: Attribution and anticipation. J Clim 30:2069–2088. https://doi.org/10.1175/JCLI-D-16-0473.1
Wang M, Overland JE (2015) Projected future duration of sea-ice-free season in the Alaskan Arctic. Prog Oceanogr 136:50–59. https://doi.org/10.1016/j.pocean.2015.01.001
Wang J, Zhang J, Watanabe E, Ikeda M, Mizobata K, Walsh JE, Bai X, Wu B (2009) Is the dipole anomaly a major driver to record lows in Arctic summer sea ice extent. Geophys Res Lett 36:L05706. https://doi.org/10.1029/2008GL036706
Wang K, Zhang T, Zhang X, Clow GD, Jafarov EE, Overeem I, Romanovsky V, Peng X, Cao B (2017) Continuously amplified warming in the Alaskan Arctic: Implications for estimating global warming hiatus. Geophys Res Lett 44:9029–9038. https://doi.org/10.1002/2017GL074232
Wang M, Yang Q, Overland JE, Stabeno P (2018) Sea-ice cover timing in the Pacific Arctic: the present and projections to mid-century by selected CMIP5 models. Deep-Sea Res II 152:22–34. https://doi.org/10.1016/j.dsr2.2017.11.017
Wood KR, Overland JE, Salo SA, Bond NA, Williams WJ, Dong X (2013) Is there a "new normal" climate in the Beaufort Sea? Polar Res 32:19552. https://doi.org/10.3402/polar.v32i0.19552
Wood KR, Bond NA, Danielson SL, Overland JE, Salo SA, Stabeno PJ, Whitefield J (2015) A decade of environmental change in the Pacific Arctic region. Prog Oceanogr 136:12–31

Wood KR, Jayne SR, Mordy CW, Bond N, Overland JE, Ladd C, Stabeno PJ, Ekholm AK, Robbins PE, Schreck MB, Heim R, Intrieri J (2018) Results of the first Arctic Heat Open Science Experiment. Bull Am Meteorol Soc 99:513–520. https://doi.org/10.1175/BAMS-D-16-0323.1

Woodgate RA (2018) Increases in Pacific inflow to the Arctic from 1990 to 2015, insights into seasonal trends and driving mechanisms from year-round Bering Strait mooring data. Prog Oceanogr 160:124–154. https://doi.org/10.1016/j.pocean.2017.12.007

Woodgate RA, Weingartner T, Lindsay R (2010) The 2007 Bering Strait oceanic heat flux and anomalous Arctic sea-ice retreat. Geophys Res Lett 37:L01602. https://doi.org/10.1029/GL041621

Woodgate RA, Stafford KM, Prahl FG (2015) A synthesis of year-round interdisciplinary mooring measurements in the Bering Strait (1990–2014) and the RUSALCA years (2004–2011). Oceanography 28:46–67. https://doi.org/10.5670/oceanog.2015.57

Yarnal B (1993) Synoptic climatology in environmental analysis: a primer. Belhaven Press, London, 195 pp

Zib B, Dong X, Xi B, Kennedy A (2012) Evaluation and intercomparison of cloud fraction and radiative fluxes in recent reanalyses over the Arctic using BSRN surface observations. J Clim 25:2291–2305. https://doi.org/10.1175/JCLI-D-11-00147.1